Nikola R. Slavkovic

Teaching Assistant
University of Belgrade
Faculty of Mechanical Engineering

Dragan S. Milutinovic

Full Professor
University of Belgrade
Faculty of Mechanical Engineering

Branko M. Kokotovic

Teaching Assistant
University of Belgrade
Faculty of Mechanical Engineering

Milos M. Glavonjic

Full Professor
University of Belgrade
Faculty of Mechanical Engineering

Sasa T. Zivanovic

Assistant Professor
University of Belgrade
Faculty of Mechanical Engineering

Kornel F. Ehmann

Full Professor
Northwestern University
Department of Mechanical Engineering

Cartesian Compliance Identification and Analysis of an Articulated Machining Robot

The application of industrial robots for machining is currently limited to tasks with low precision demands due to the low stiffness of industrial robots as compared to machine tools. This paper analytically describes an experiment-based compliance identification and analysis method for a 5-axis vertical articulated machining robot. An expansion of the conventional method for the calculation of the robot's Cartesian space compliance that takes into consideration joint compliances and the Jacobian matrix is used. The analytical analysis considers the effects of the individual joint compliances on the resulting Cartesian space compliance. Experimentally, the Cartesian space compliance is obtained by direct measurement of the absolute displacements induced by static forces along 3-Cartesian directions at the tool tip from which the joint compliances are identified.

Keywords: machining robot, compliance identification, compliance analysis.

1. INTRODUCTION

Industrial robots are promising cost-effective and flexible alternatives for certain multi-axis milling applications. Compared to machine tools, industrial robots are cheaper and more flexible with a potentially larger workspace. For these reasons, researchers, robot and CAM software manufacturers as well as people from machining shops find it feasible to replace machine tools by robots for some machining applications. It is well known that poor accuracy, stiffness and the complexity of programming are the most important limiting factors for wider adoption of robotic machining in machine shops [1,2].

Stiffness modelling, analysis, synthesis and control in robotic machining have attracted the attention of many researchers. As stated in [2] the major position error sources in robotic machining can be classified into two categories: (i) cutting force induced errors, and (ii) motion errors (e.g., kinematic, dynamic, etc.).

Motion errors, typically in the range of 0.1 mm, are inherent and rooted in the robot's position controller, and they would appear even in non-contact tasks. As milling cutting forces are of several hundred N, the force–induced errors could easily exceed 1 mm. The latter statement is quite logical because the stiffness for typical articulated robots is usually less than 1 N/μm, while standard CNC machine tools often have stiffness values greater than 50 N/μm. Similar statements are also given in [3].

The sources that determine the stiffness of a typical robot manipulator are the compliance of its joints, actuators and other transmission elements, geometric and material properties of the links, base, and the active stiffness provided by its position control system. For the purpose of this research, we assume that the compliance of the actuators and of the transmission elements is the dominant source of the stiffness, and it can be represented by a linear torsional spring for each joint, while the links are infinitely stiff. The active compliance of the actuators due to the robot's position control system, provided by the original equipment manufacturer, does not vary with time although an integral controller can increase the active compliance, depending on the positioning error [4].

Unlike multi-axis CNC machine tools, robot tool tip displacements are coupled and vary even when subjected to the same force at different workspace locations. Such coupling results in displacements not only in the direction of the reaction force, but can also generate some counter-intuitive results. Mainly, three kinds of deviations occur due to the compliance of a machining robot during high speed cutting: static displacements, low frequency and high frequency oscillations [5].

In this paper, the static displacements which have the highest impact on overall cutting accuracy are analysed.

In order to contribute to efficient use of robots for machining applications, research and development of reconfigurable robotic machining systems was initiated [6] that considers two classes of problems. The first relates to the realization of a specialized 5-axis vertical articulated machining robot with an integrated motor spindle in order to improve robotic machining accuracy. The second refers to the development of the machining

robot's control and programming system which can be directly used by CNC machine tool programmers and operators [7].

In order to obtain the Cartesian space compliance matrix of the 5-axis vertical articulated machining robot, two methods, similar to [8], were used in this paper. The first method is an analytically-based approach that calculates the Cartesian space compliance using joint compliances and the Jacobian matrix [9,10].

In this method, only five experiments are required to evaluate the robot's Cartesian space compliance matrix throughout its workspace. This conventional method is expanded in the present paper with the aim of analyzing the effects of the compliance of each individual joint on the robot's Cartesian space compliance. The analysis of compliance effects of each individual joint on the Cartesian space compliance could be of crucial importance for a robot manufacturer's experts in the design of specialized machining robots.

The second method obtains the robot's Cartesian space compliance matrix throughout its workspace by direct measurement of the absolute displacements of the tool-tip induced by static forces along 3-Cartesian directions. This method improves the results of the analytical method, because it takes into account all deformations including the joint and link flexibilities along and about all the axes, however, it requires a large number of measurements.

2. PROBLEM STATEMENT

A basic module of the proposed concept of the robotic machining system presented in [7] is the specialized 5-axis vertical articulated robot, Figure 1, with an integrated motor spindle, similar to [8, 11] and with a larger workspace, higher payload and stiffness. The development of the specialized 5-axis vertical articulated machining robot was a joint project with a robot manufacturer.

For the compliance identification and analysis a six-axis vertical articulated robot, Figure 1, was used as a testbed in the way that axis number six was blocked. The robot is equipped with a high speed motor spindle with the maximal speed of 18,000 min⁻¹.
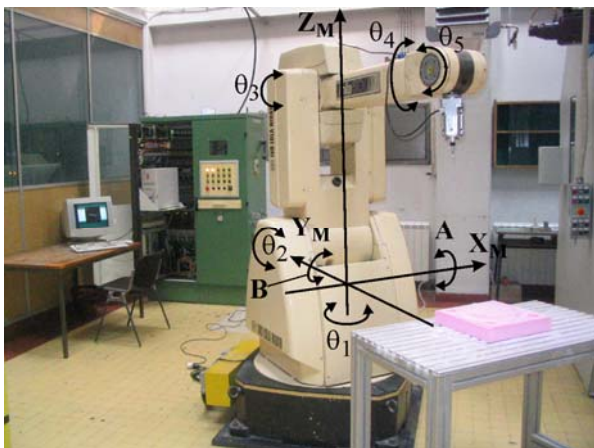
Figure 1. The experimental 5-axis machining robot in reference position

As evident from Figure 1, the experimental five-axis machining robot is further considered as a five-axis vertical milling machine (X, Y, Z, A, B) of the spindle-tilting type [12], where machining is performed on a work table in front of the robot. The configured system as well as the limited motions in joints relative to the reference position provide for: (i) conveniences related to stiffness [1], (ii) taking into account only one solution of the inverse kinematics, and (iii) avoiding the robot's singularities [13].

The focus of the current research, one part of the results being presented in this paper, is related to compliance identification and analysis of the experimental 5-axis vertical articulated machining robot, which includes: (i) an analytically-based Cartesian compliance identification, (ii) an experimentally-based Cartesian compliance identification, and (iii) machining experiments.

3. KINEMATIC MODELING

As it was mentioned, the 5-axis vertical articulated robot in Figure 1 will be considered below as a specific configuration of a 5-axis spindle-tilting type vertical milling machine (X, Y, Z, A, B). Figure 2 represents the kinematic model of the robot.

The robot reference frame {M} has been adopted according to the standard for this machine type [14] and coincides with the robot's base frame (x_0, y_0, z_0). The tool frame {T} is attached to the milling tool tip, T, in a way that the z_T axis coincides with the tool axis and also coincides with the axis of the last link of the robot to which the motor spindle is attached. Vector **v,** referenced in frame {M}, is denoted by $^M\mathbf{v}$.
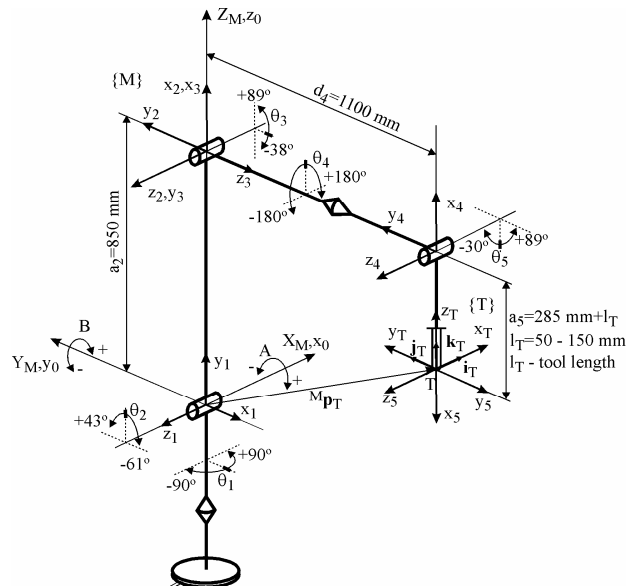
Figure 2. Kinematic model of the robot

The joint coordinate vector for this 5-axis vertical articulated robot is represented by:

$$\mathbf{\theta} = \begin{bmatrix} \theta_1 & \theta_2 & \theta_3 & \theta_4 & \theta_5 \end{bmatrix}^T \qquad (1)$$

where θ_i, $i = 1,2,...,5$ are scalar joint variables controlled by the actuators.

Given that the robot has 5 DOF, only the direction of the tool's z_T axis is controllable, while axes x_T and y_T will have uncontrollable rotations about it. The position and orientation of the tool frame, {T}, relative to the robot's reference frame, {M}, is given by the homogeneous coordinate transformation matrix [15, 16]:

$$^M_T T = \left[\begin{array}{ccc|c} & ^M_T R & & ^M\mathbf{p}_T \\ \hline 0 & 0 & 0 & 1 \end{array}\right] =$$

$$= \left[\begin{array}{ccc|c} i_{Tx} & j_{Tx} & k_{Tx} & X_M \\ i_{Ty} & j_{Ty} & k_{Ty} & Y_M \\ i_{Tz} & j_{Tz} & k_{Tz} & Z_M \\ \hline 0 & 0 & 0 & 1 \end{array}\right] \quad (2)$$

where the position vector $^M\mathbf{p}_T$ represents the position, while $^M_T R$ represents the orientation of the tool frame, {T}, with respect to the robot's reference frame, {M}. As only the orientation of the tool axis z_T specified by the unit vector $^M\mathbf{k}_T = [k_{Tx}\ k_{Ty}\ k_{Tz}]^T$ is of interest, equation (2), the tool orientation angles, A and B, can be determined in the usual way [7, 12, 15], so that the world coordinate vector can be expressed as:

$$\mathbf{x} = \begin{bmatrix} X_M & Y_M & Z_M & A & B \end{bmatrix}^T \quad (3)$$

3.1 Jacobian matrix

To model the robot, the Denavit-Hartenberg (D-H) notation [15, 16] is used. To perform the kinematic analysis, first the coordinate frames are rigidly attached to each link, Figure 2. The homogeneous transformation describing the relation between links is traditionally referred to as an A matrix.

The matrix $^{i-1}_i A$ designates the D-H transformation matrix relating frame (i) to frame (i-1). Figure 2 shows the D-H coordinate frames for the 5-axis robot from Figure 1 in the reference position, taking into account the ranges of joint motions.

The D-H model adopts 4 parameters (ai, αi, di, θi) to describe the transformation, including translations and rotations from link (i-1) to link (i). After the D-H coordinate frame is assigned to each link, the transformation between successive frames (i-1) and (i) is described as follows:

$$^{i-1}_i A = Rot(z_{i-1}, \theta_i) \cdot Trans(0,0,d_i) \cdot Trans(a_i,0,0) \cdot Rot(x_i, \alpha_i) =$$

$$\quad (4)$$

$$= \left[\begin{array}{ccc|c} ^{i-1}\mathbf{i}_i & ^{i-1}\mathbf{j}_i & ^{i-1}\mathbf{k}_i & ^{i-1}\mathbf{p}_{Oi} \\ \hline 0 & 0 & 0 & 1 \end{array}\right]$$

Considering the above-mentioned remarks and constraints, a list of D-H kinematic parameters for each link is given in Table 1.

Table 1. D-H kinematic parameters

link i	$\alpha_i[°]$	$a_i[mm]$	$d_i[mm]$	$\theta_i[°]$
1	90	0	0	θ_1-90
2	0	a_2	0	θ_2+90
3	90	0	0	θ_3
4	-90	0	d_4	$-\theta_4$
5	0	a_5	0	θ_5+180

Substituting the D-H parameters of the links into equation (4) the transformation matrices $^{i-1}_i A$, $i = 1,2,...,5$ are obtained first. Considering that the robot is considered in the present paper as a 5-axis spindle-tilting type vertical milling machine (X, Y, Z, A, B), importance is given to frame {T} whose z_T axis must coincide with the tool axis. As noticeable from Figure 2, frame {T} can be described relative to the frame (x_5, y_5, z_5) by the homogeneous transformation matrix $^5_T T$.

Now, as it is well-known [15, 16], the tool position and orientation, i.e., the position and orientation of frame {T} with respect to the robot's reference frame {M}, Figure 1, for the given joint coordinates vector θ and specified link parameters can be determined as:

$$^M_T T = ^0_1 A \cdot ^1_2 A \cdot ^2_3 A \cdot ^3_4 A \cdot ^4_5 A \cdot ^5_T T =$$

$$= \left[\begin{array}{ccc|c} & ^M_T R & & ^M\mathbf{p}_T \\ \hline 0 & 0 & 0 & 1 \end{array}\right] = \left[\begin{array}{ccc|c} i_{Tx} & j_{Tx} & k_{Tx} & X_M \\ i_{Ty} & j_{Ty} & k_{Ty} & Y_M \\ i_{Tz} & j_{Tz} & k_{Tz} & Z_M \\ \hline 0 & 0 & 0 & 1 \end{array}\right] (5)$$

In equation (5), apart from the position of tool tip T in the reference frame {M} $^M\mathbf{p}_T = [X_M\ Y_M\ Z_M]^T$, the third column $^M\mathbf{k}_T = [k_{Tx}\ k_{Ty}\ k_{Tz}]^T$ of the rotation matrix $^M_T R$ is of significance as the robot has only 5-DOF. Considering that the robot reference frame, {M}, and the robot base frame (x_0, y_0, z_0) coincide and that the tool tip, T, is the origin of frame {T} and also the origin of frame(x_5, y_5, z_5), Figure 2, it is obvious that:

$$^M\mathbf{p}_T = {}^0\mathbf{p}_T = {}^0\mathbf{p}_{O5} \quad (6)$$

The position and orientation of an arbitrary frame (i) attached to link (i) with respect to the robot's reference frame, {M}, i.e., robot base frame (x_0, y_0, z_0) can be expressed as:

$$^M_i T = {}^0_i T = {}^0_1 A \cdot {}^1_2 A \cdots {}^{i-1}_i A = \prod_{j=1}^{i} {}^{j-1}_j A =$$

$$= \left[\begin{array}{ccc|c} & ^0_i R & & ^0\mathbf{p}_{Oi} \\ \hline 0 & 0 & 0 & 1 \end{array}\right] = \left[\begin{array}{ccc|c} ^0\mathbf{i}_i & ^0\mathbf{j}_i & ^0\mathbf{k}_i & ^0\mathbf{p}_{Oi} \\ \hline 0 & 0 & 0 & 1 \end{array}\right] \quad (7)$$

for $i = 1,2,...,n$ where $n=5$ is the number of joints.

The robot's Jacobian matrix relates joint velocities to Cartesian velocities of the tool tip. The mapping between the static forces applied at the end-effector and the resulting torques at the joints can also be described

by the Jacobian matrix [15-18]. Considering that the robot consists of five revolute joints, the Jacobian matrix has as many rows as there are degrees of freedom and the number of columns is equal to the number of joints:

$$J = \begin{bmatrix} \mathbf{J}_1 & \mathbf{J}_2 & ... & \mathbf{J}_n \end{bmatrix} \qquad (8)$$

with column vectors

$$\mathbf{J}_i = \begin{bmatrix} {}^0\mathbf{k}_{i-1} \times \left({}^0\mathbf{p}_{On} - {}^0\mathbf{p}_{Oi-1} \right) \\ {}^0\mathbf{k}_{i-1} \end{bmatrix} \qquad (9)$$

Substituting the vectors from equation (7) into equation (9) the Jacobian matrix columns Ji, i = 1,2,...,5 are obtained.

3.2 Machining robot workspace

Based on the inverse kinematics, it is possible to determine the position and orientation workspace of the robot considered here as a vertical 5-axis milling machine [7]. The position and orientation workspace are given by:

$$Ws(X_M, Y_M, Z_M, A, B) = \{0,1\} \qquad (10)$$

which represents a Boolean function, whose value is equal to 1 if the tool pose defined by the world coordinates vector **x** is reachable without exceeding the limited motion range of the joints. Starting from a selected point in the workspace volume, the determination is made by a specific step-by-step strategy that locates the tool in a given pose in the workspace and that determines whether the pose is reachable or not by taking into account the limited motion range of the joints given in Figure 2. The portion of workspace for 3-axis machining ($A=0^o$, $B=0^o$, i.e., spindle orientation is perpendicular to the $X_M Y_M$ plane) with boundaries logical for machining (Z_{Mmin}=-400 mm, Z_{Mmax}=100 mm) is shown in Figure 3. For programmers and operators familiar with CNC machine tools, this workspace is reduced to the parallelepiped X_MxY_MxZ_M = 1200x600x500 mm^3, as indicated in Figure 3.
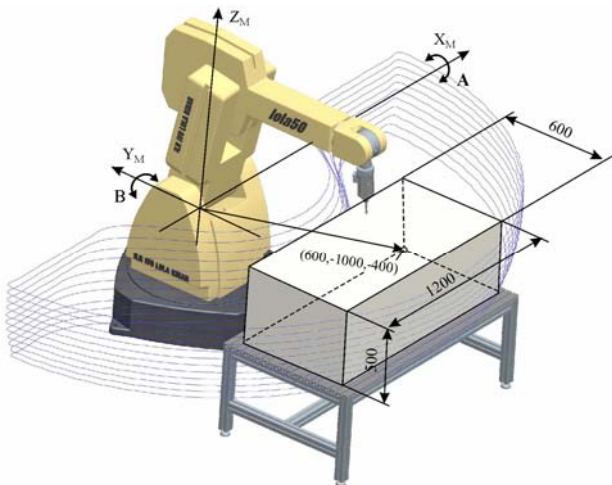
Figure 3. Workspace in the case of 3-axis machining (A=0°, B=0°)

As it is known [15, 18], det(J) represents the manipulability measure usually adopted as a distance of the robot from its singular configurations. Figure 4 shows the distributions of the values of det(J) in the planes Z_M=-400mm *and* Z_M=100mm in the adopted portion of the workspace X_MxY_MxZ_M = 1200x600x500 mm^3.
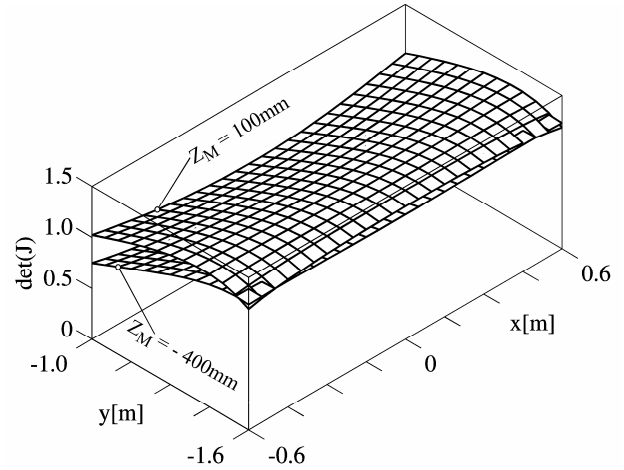
Figure 4. Distributions of det(J) values in the planes Z_M=-400 mm and Z_M=100 mm

Similar distributions of the values of *det(J)* are also found in the planes from Z_M=-400 mm to Z_M=100 mm. The presented distributions of the values for *det(J)* exhibit good force and speed transmission ratios of the tool with driving forces and speeds throughout the selected portion of the workspace.

4. ANALYTICALLY-BASED CARTESIAN COMPLIANCE IDENTIFICATION

The knowledge of the robot's stiffness or compliance reflected at its end point is of prime importance to successfully conduct contact and noncontact tasks [4]. As stated in [2,3,8,19] the elastic properties of the robot's links are insignificant, so the subsequent analysis of the compliance model in Cartesian space will be based on joint compliances. The analysis will be conducted on the existing experimental machining robot shown in Figure 1 as a basis for realizing the machining robot concept with integrated motor spindle from Figure 1.

The Cartesian compliance model should allow for generating the robot's compliance maps which indicate the robot's end point compliance as a function of the joint compliances and robot configurations throughout its workspace.

Based on the principle of virtual work, the conventional formulation for the mapping of the joint compliance matrix, C_θ, into the Cartesian space compliance matrix, $C_X(\mathbf{\theta})$, is expressed as [8-10]:

$$C_X(\mathbf{\theta}) = J(\mathbf{\theta}) \cdot C_\theta \cdot J(\mathbf{\theta})^T \qquad (11)$$

where C_θ is a constant matrix of diagonal form:

$$C_\theta = diag(C_{\theta 1},...,C_{\theta n}) \qquad (12)$$

and $J(\theta)$ is the Jacobian matrix given by equation (8).

The practical application of equation (11) to determine the robot's compliance center and the machining robot's compliance analysis were presented in [10] and [8]. It was shown how suitable it is, for it allows the mapping of the joint compliance matrix C_θ into the Cartesian compliance matrix $C_X(\theta)$ without calculating any inverse kinematic functions.

Since C_θ is diagonal, the Cartesian space compliance matrix $C_X(\theta)$, equation (11), in this paper is considered as the sum of the joint compliances associated with each individual joint as:

$$C_X(\theta) = C_{X1}(C_{\theta 1}) + ... + C_{Xn}(C_{\theta n}) = \sum_{i=1}^{n} C_{Xi}(C_{\theta i}) \quad (13)$$

where

$$C_{Xi}(C_{\theta i}) = C_{\theta i} \cdot \mathbf{J}_i \cdot \mathbf{J}_i^T =$$

$$C_{\theta i} \cdot \begin{bmatrix} J_{1i} \cdot J_{1i} & J_{1i} \cdot J_{2i} & J_{1i} \cdot J_{3i} & J_{1i} \cdot J_{4i} & J_{1i} \cdot J_{5i} \\ J_{2i} \cdot J_{1i} & J_{2i} \cdot J_{2i} & J_{2i} \cdot J_{3i} & J_{2i} \cdot J_{4i} & J_{2i} \cdot J_{5i} \\ J_{3i} \cdot J_{1i} & J_{3i} \cdot J_{2i} & J_{3i} \cdot J_{3i} & J_{3i} \cdot J_{4i} & J_{3i} \cdot J_{5i} \\ J_{4i} \cdot J_{1i} & J_{4i} \cdot J_{2i} & J_{4i} \cdot J_{3i} & J_{4i} \cdot J_{4i} & J_{4i} \cdot J_{5i} \\ J_{5i} \cdot J_{1i} & J_{5i} \cdot J_{2i} & J_{5i} \cdot J_{3i} & J_{5i} \cdot J_{4i} & J_{5i} \cdot J_{5i} \end{bmatrix}, \quad (14)$$

$$i = 1,2,...,n, \ n = 5$$

represents a part of Cartesian space compliance matrix $C_X(\theta)$ originating from the i-th joint compliance $C_{\theta i}$, while $\mathbf{J}_i$ are column vectors given by equation (9).

Equations (13) and (14) provide insight into the effects of the compliance of each individual joint on the Cartesian space compliance. This means that the effect of the corresponding joint is obtained by incorporating into equation (13) only its compliance, while the other joints are considered stiff. This is of crucial importance for the present paper, because it can be useful for a robot manufacturer's experts in the design of specialized machining robots.

For an articulated robot, $C_X(\theta)$ is a symmetric non-diagonal and configuration dependent matrix. The force and robot tool tip displacement in Cartesian space is coupled, which means that the force applied in one direction will cause displacements in all possible directions.

Compliance is also a function of the robot's Jacobian matrix $J(\theta)$ that changes significantly throughout the entire workspace. Thus, if C_θ can be experimentally determined, the Cartesian space compliance matrix $C_X(\theta)$, equation (11) and the linear displacement of the robot's tool tip $\delta\mathbf{x} = [\delta x \ \delta y \ \delta z]^T$ under an external static force vector $\mathbf{F} = [Fx \ Fy \ Fz]^T$ at any location in the workspace can be estimated as:

$$\delta\mathbf{x} = C_{X\delta}(\theta) \cdot \mathbf{F} = \begin{bmatrix} Cxx & Cxy & Cxz \\ Cyx & Cyy & Cyz \\ Czx & Czy & Czz \end{bmatrix} \cdot \mathbf{F} \quad (15)$$

where $C_{X\delta}(\theta)$ is a submatrix of Cartesian space compliance matrix $C_X(\theta)$. In equation (15) direct- and cross-compliance can be calculated using equations (13) and (14) us:

$$C_{xx} = \sum_{i=1}^{5} C_{\theta i} \cdot J_{1i}^2 \qquad C_{xy} = \sum_{i=1}^{5} C_{\theta i} \cdot J_{1i} \cdot J_{2i}$$

$$C_{xz} = \sum_{i=1}^{5} C_{\theta i} \cdot J_{1i} \cdot J_{3i} \qquad C_{yx} = \sum_{i=1}^{5} C_{\theta i} \cdot J_{2i} \cdot J_{1i}$$

$$C_{yy} = \sum_{i=1}^{5} C_{\theta i} \cdot J_{2i}^2 \qquad C_{yz} = \sum_{i=1}^{5} C_{\theta i} \cdot J_{2i} \cdot J_{3i}$$

$$C_{zx} = \sum_{i=1}^{5} C_{\theta i} \cdot J_{3i} \cdot J_{1i} \qquad C_{zy} = \sum_{i=1}^{5} C_{\theta i} \cdot J_{3i} \cdot J_{2i}$$

$$C_{zz} = \sum_{i=1}^{5} C_{\theta i} \cdot J_{3i}^2 \qquad (16)$$

The experimental determination of the compound joint compliance parameters is critical for the robot's compliance analysis. For the measurement of each joint's compliance the robot structure was not disassembled.

To assure the decoupling of the joints only one joint at a time was loaded [8]. Therefore, while measuring the compliance of joint (i) all joints from the base to joint (i-1) were blocked. Table 2 shows the experimentally identified compound joint compliances.

Table 2. Experimentally identified joint compliances

Joint number i	1	2	3	4	5
Compliance $C_{\theta i}$ [rad/Nm]·10^{-7}	7.14	10.12	12.30	17.32	91.35

4.1 Analytical results

Using equation (16) and the experimentally identified compound joint compliances, Table 2, the direct- and cross-compliances were calculated in the adopted workspace shown in Figure 3.

Figure 5 shows the distribution of the analytically determined compliances in the Z_M=0 plane. The distributions of direct-compliances C_{xx}, C_{yy}, and C_{zz} are presented in Figures 5a, 5e, and 5i respectively.

The distributions of cross-compliances C_{yx}, C_{zx}, and C_{zy} are given in Figures 5b, 5c, and 5f respectively. Figure 5 can be also viewed as the Cartesian space compliance matrix $C_X(\theta)$ in the Z_M=0 plane in the adopted workspace shown in Figure 3.
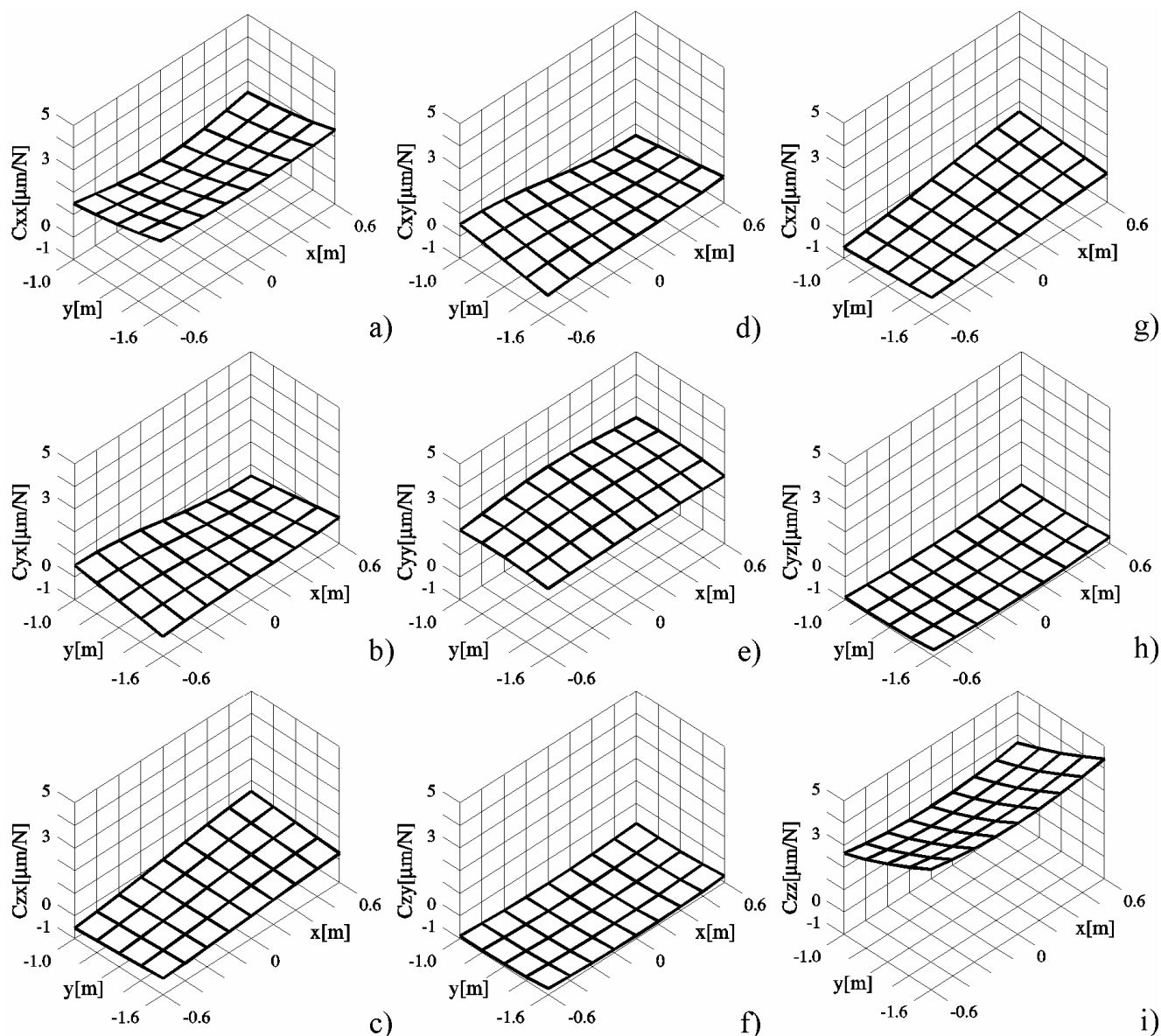
Figure 5. Distributions of analytically determined compliances in the plane $Z_M=0$

As it is noticeable from Figures 5a and 5i, the direct-compliances C_{xx} and C_{zz} are decreasing in the positive Y_M direction. At constant Y_M positions the direct-compliances C_{xx} and C_{zz} are increasing in the negative and positive X_M directions. The direct-compliance C_{yy}, Figure 5e, is increasing in the positive Y_M direction and decreasing in the negative and positive X_M directions at a constant Y_M positions.

The distributions of the all components of the direct-compliances originating from individual joints, summands in equation (16), are shown in Figure 6. The direct-compliances C_{xx} and C_{yy}, Figures 6a and 6b, are predominantly affected by joint compliances $C_{\theta 1}$, $C_{\theta 3}$, and $C_{\theta 5}$. The direct-compliance C_{zz}, Figure 6c, is predominantly affected only by joint compliances $C_{\theta 2}$ and $C_{\theta 3}$.

In order to complete the impact analysis of compliances of each joint, this paper also considers their impact on cross-compliances.

The distributions of the all components of the cross-compliances originating from individual joints, summands in equation (16), are shown in Figure 7.

The cross-compliance C_{xy}, Figure 7a, is predominantly affected by joint compliances $C_{\theta 1}$, $C_{\theta 3}$, and $C_{\theta 5}$, while cross-compliances C_{xz}, Figure 7b, and C_{zy}, Figure 7c, are predominantly affected only by the joint compliance $C_{\theta 3}$.

4.2 Simulation of the tool path errors calculated from the analytically determined Cartesian compliance

To test the effectiveness of analytically based compliance model as well as to analyze tool path errors based on it, simple tasks were chosen. Programmed linear paths parallel to the X_M and Y_M axes are shown in Figures 8a and 8b respectively.
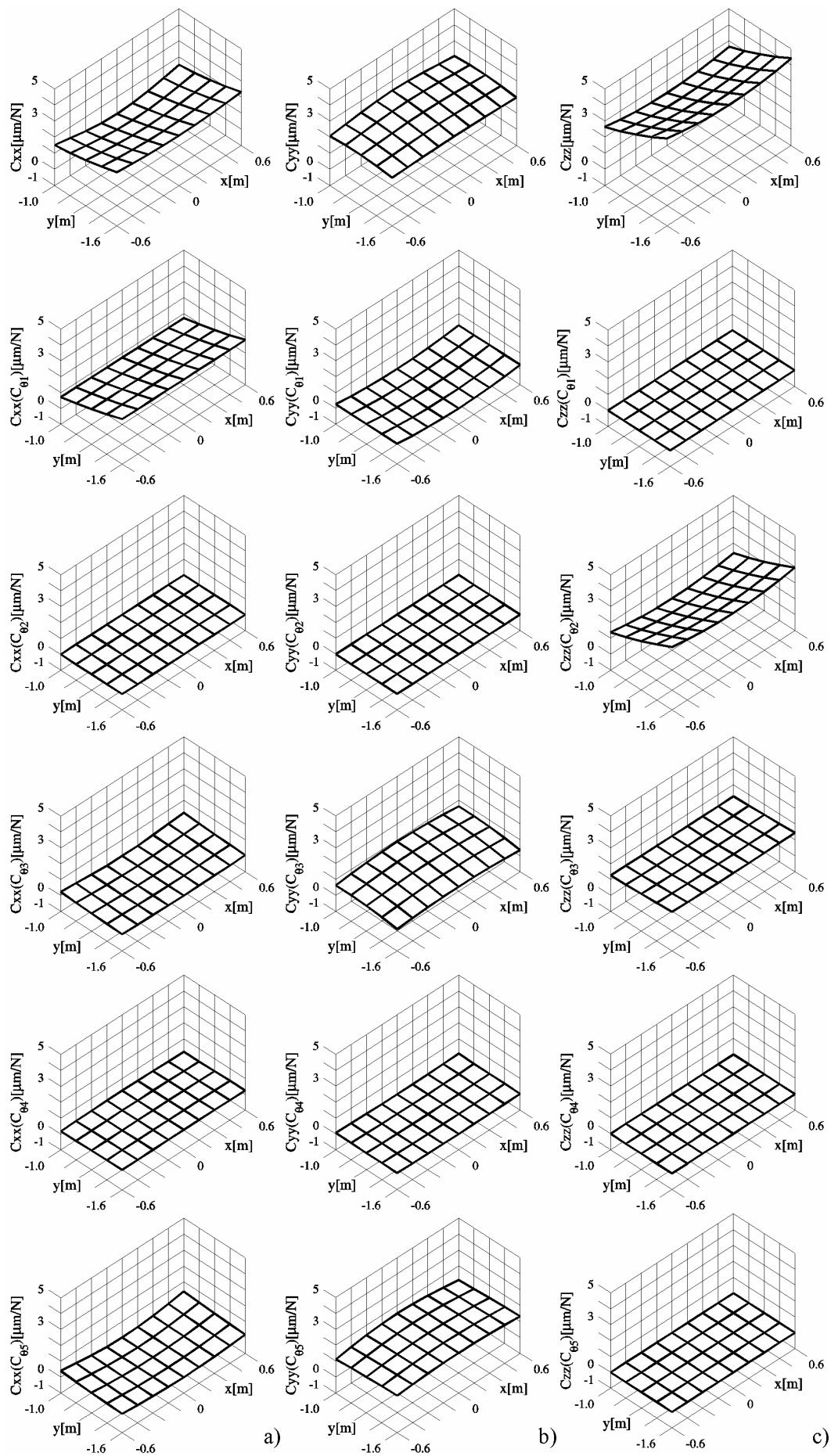
Figure 6. Distributions of analytically determined direct-compliances' components
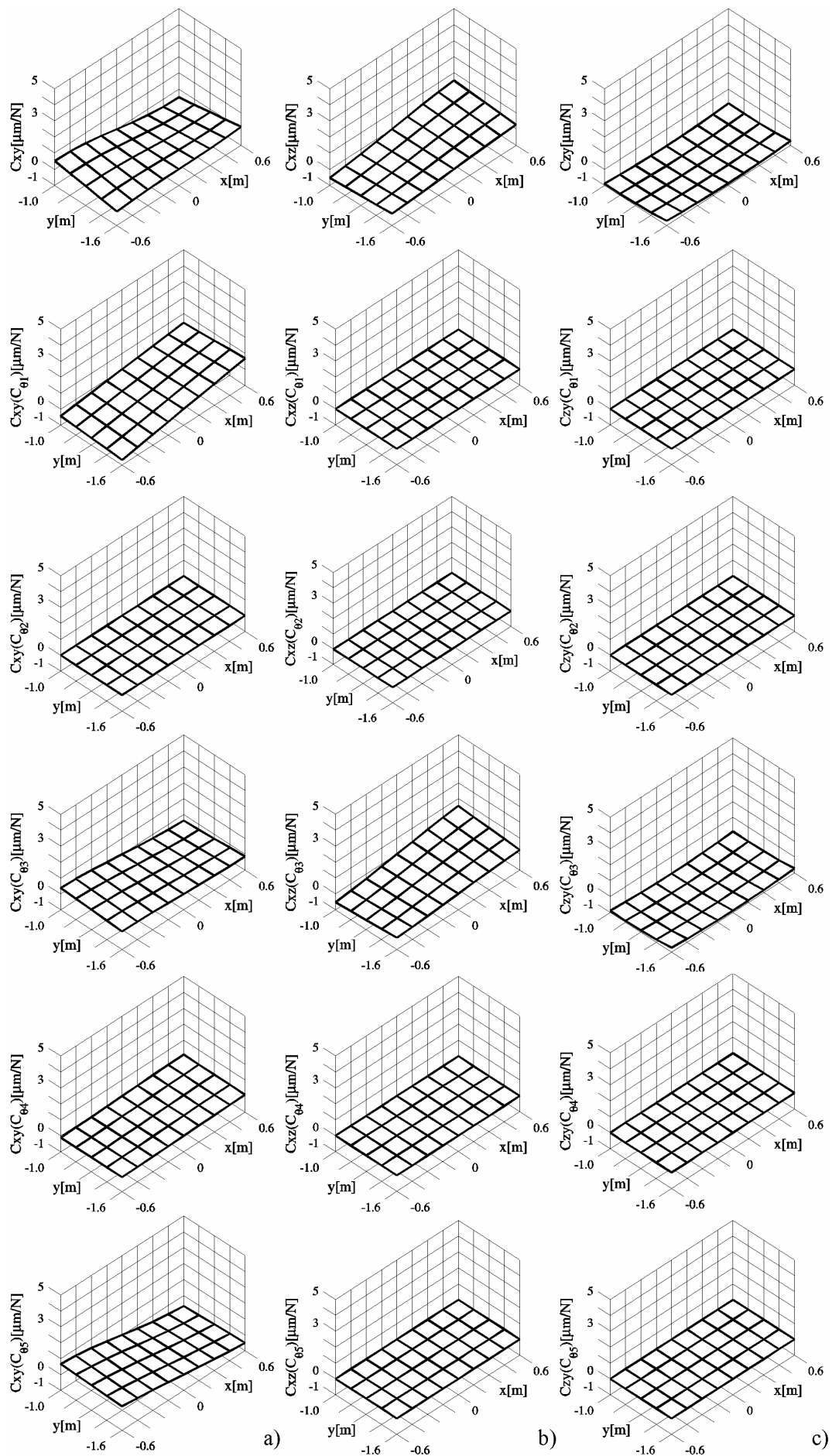
Figure 7. Distributions of analytically determined cross-compliances' components
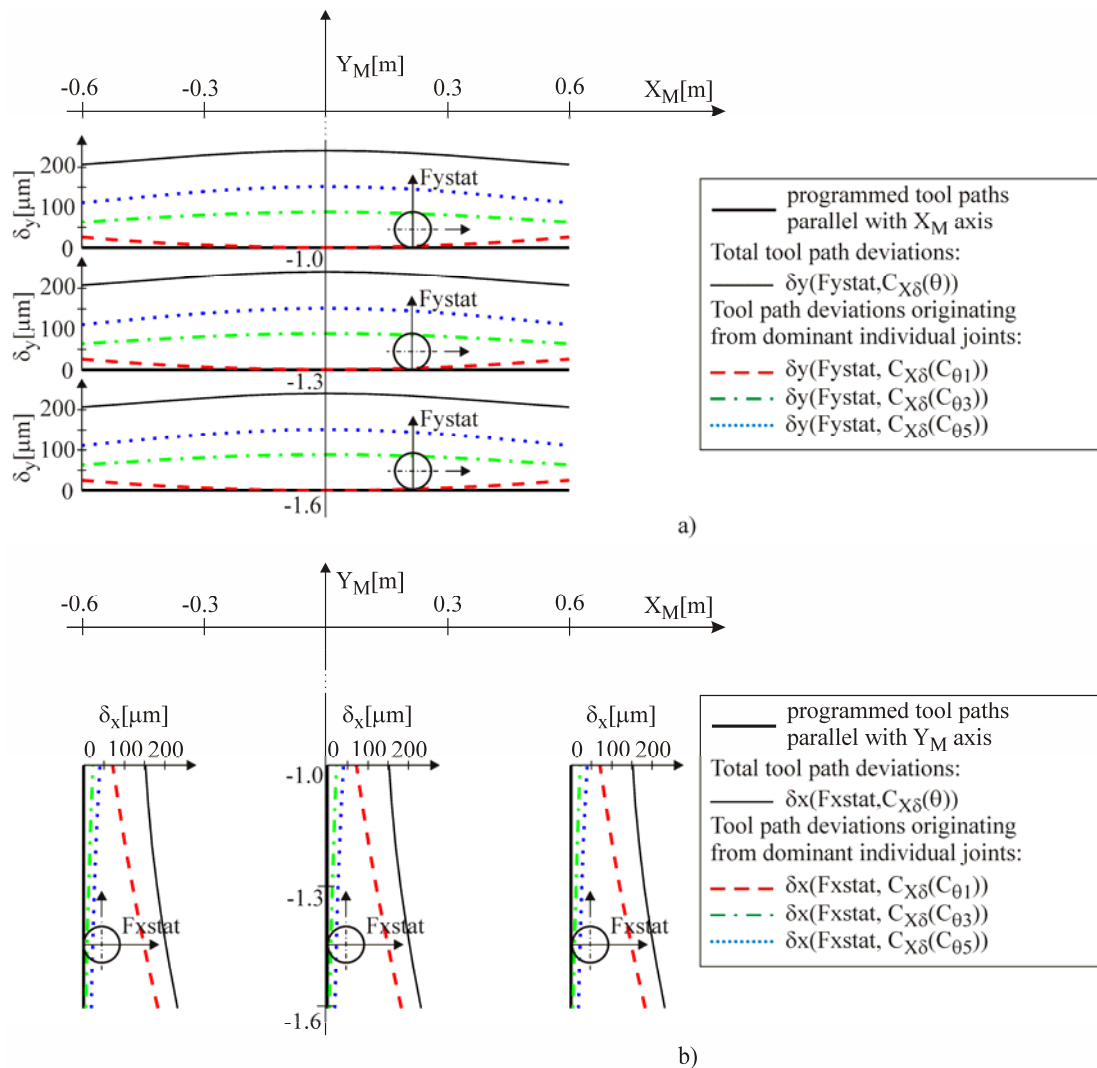
Figure 8. Tool path deviations in the plane $Z_M=0$

Selected linear paths are on the borders and in the middle of adopted portion of the workspace in the plane Z_M=0mm. The total tool path deviations as well as the tool path deviations originating from the dominant individual joints' compliances are calculated for the constant static forces in the feed normal directions, i.e., *Fxstat = Fystat* = 100N. Similar tool path deviations are also obtained in the planes from Z_M=-400 mm to Z_M=100 mm. From these simple simulation examples it can be easily concluded that it is possible to generate compliance-induced machining error maps and identify critical joints and workspace sub-volumes in an efficient way using an analytically-based compliance model.

5. EXPERIMENTALLY-BASED CARTESIAN COMPLIANCE IDENTIFICATION

Another approach to obtain the Cartesian compliance of the machining robot is the direct measurement of the absolute displacements induced by a load at the tool tip. The elements of the experimental setup shown in Figure 9 are the experimental machining robot (1) equipped with a sphere-tip tool (2), fixture (3), cable-pulley system (4) and a deadweight of 250 N (5) in order to

exert static forces along 3 Cartesian directions at the sphere-tip tool. The original and deformed positions of the sphere-tip tool are measured by a FARO Portable CMM 3D digitizer (6), from which translational displacements $\delta x, \delta y,$ and δz are calculated.
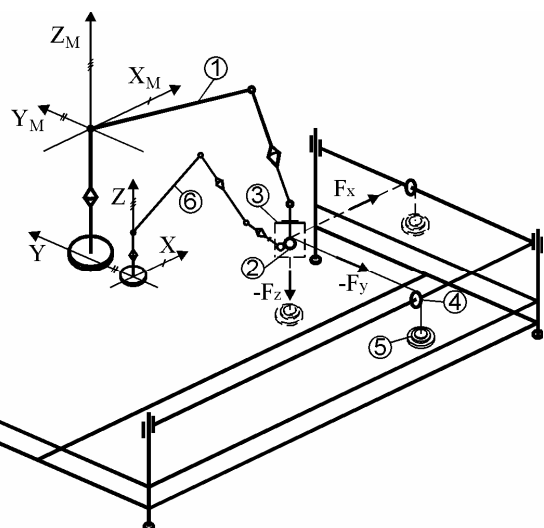
Figure 9. Scheme of robot loading and displacements measurement

For the analysis of the Cartesian compliance investigations were conducted within the adopted portion of the workspace X_MxY_MxZ_M = 1200x600x500 mm³, Figure 3. The workspace was subdivided into smaller cubes and the displacements of the sphere-tip tool were measured at 45 points at 6 Z_M levels (Z_M=-400 to 100 mm).

Figure 10. Experimental setup of robot loading and displacements measurement

The experiment-based compliances are determined on the basis of the sphere-tip tool's displacements $\delta x, \delta y,$ and δz induced by static forces of 250 N in all 3 Cartesian directions. An example of displacement measurements for the cases of robot loading in the negative Y_M direction is shown in Figure 10.

5.1 Experimental results

Direct- and cross-compliances were calculated from the measured displacements as:

$$C_{xx} = \delta x(Fx)/Fx \qquad\qquad C_{xy} = \delta x(Fy)/Fy$$

$$C_{xz} = \delta x(Fz)/Fz \qquad\qquad C_{yx} = \delta y(Fx)/Fx$$

$$C_{yy} = \delta y(Fy)/Fy \qquad\qquad C_{yz} = \delta y(Fz)/Fz$$

$$C_{zx} = \delta z(Fx)/Fx \qquad\qquad C_{zy} = \delta z(Fy)/Fy$$

$$C_{zz} = \delta z(Fz)/Fz \qquad\qquad\qquad (17)$$

The distributions of direct-compliances C_{xx}, C_{yy}, and C_{zz} are shown in Figures 11a, 11e and 11i respectively. The distributions of cross-compliances C_{yx}, C_{zx}, C_{xy}, C_{zy}, C_{xz} and C_{yz} are shown in Figures 11b, 11c, 11d, 11f, 11g and 11h respectively.
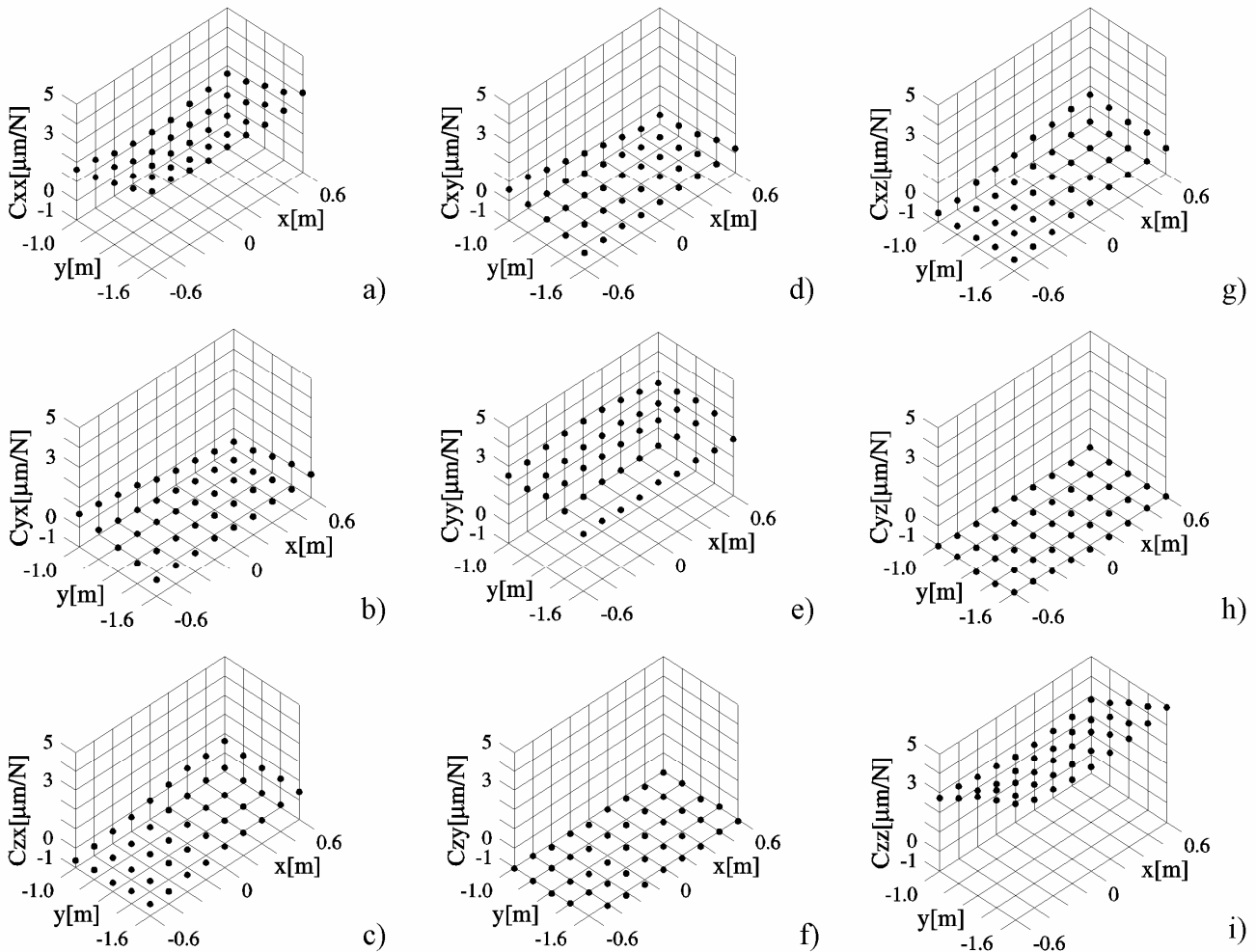
Figure 11. Distributions of experimentally determined compliances in the ZM=0 plane

Comparing the experimental with the analytically determined compliances, Figure 5, it can be inferred that the character of their distributions is similar, but the experimentally obtained compliances are slightly higher. The higher values of the experimentally obtained compliances compared to those determined analytically originate from the compliance of the structural elements, motor spindle and the tool itself.

In order to identify the joint compliances $C_{\theta i}$, i=1,2,...,5 the experimentally determined direct- and cross-compliances form equation (17) can be substituted in equation (16). For example, at the selected nine points (T1-T9), shown in Figure 12, an over-determined system of 81 equations was derived from which the joint compliances $C_{\theta i}$, i=1,2,...,5 were identified using the Matlab function lsqcurvefit. Table 3 shows the determined joint compliances.
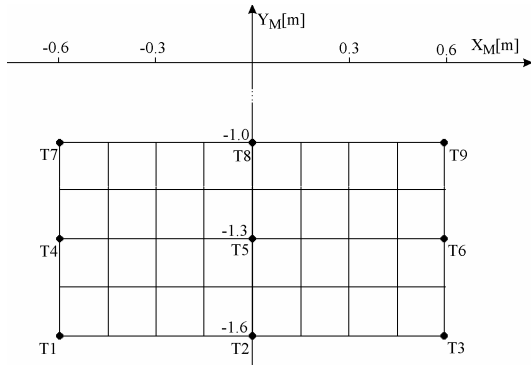
Figure 12. Selected points in the Z_M=0 plane for joint compliance identification

Table 3. Joint compliances identified based on experimental Cartesian compliances in the Z_M=0 plane

Joint number i	1	2	3	4	5
Compliance $C_{\theta i}$ [rad/Nm]·10^{-7}	9.03	11.17	14.74	27.65	97.58

With the identified joint compliances, Table 3, the Cartesian space compliance submatrix $C_{X\delta}(\boldsymbol{\theta})$ was calculated again using equation (16). Figure 13 shows the distributions of the calculated direct- and cross-compliances in the Z_M=0 plane based on the identified joint compliances given in Table 3. The distributions of experimentally determined compliances from Figure 11 are also shown in Figure 13.

Comparing the joint compliances identified based on experimental Cartesian compliances, Table 3, with experimentally identified joint compliances from Table 2 it can be inferred that their values are slightly higher.

5.2   Milling test

Milling tests were carried out on aluminum workpieces placed on a 3-component dynamometer (D), Figure 14. The programmed linear path was in the plane Z_M= 0 in the positive X_M direction around the point (X_M = 0 mm, Y_M = -1300 mm). The tool used was a three-flute flat endmill with a diameter of 8 mm. The milling operation was endmilling with a cutting width of 8 mm, depth of cut 2 mm, spindle speed 12,000 min^{-1}, and feed velocity 30 mm/s.
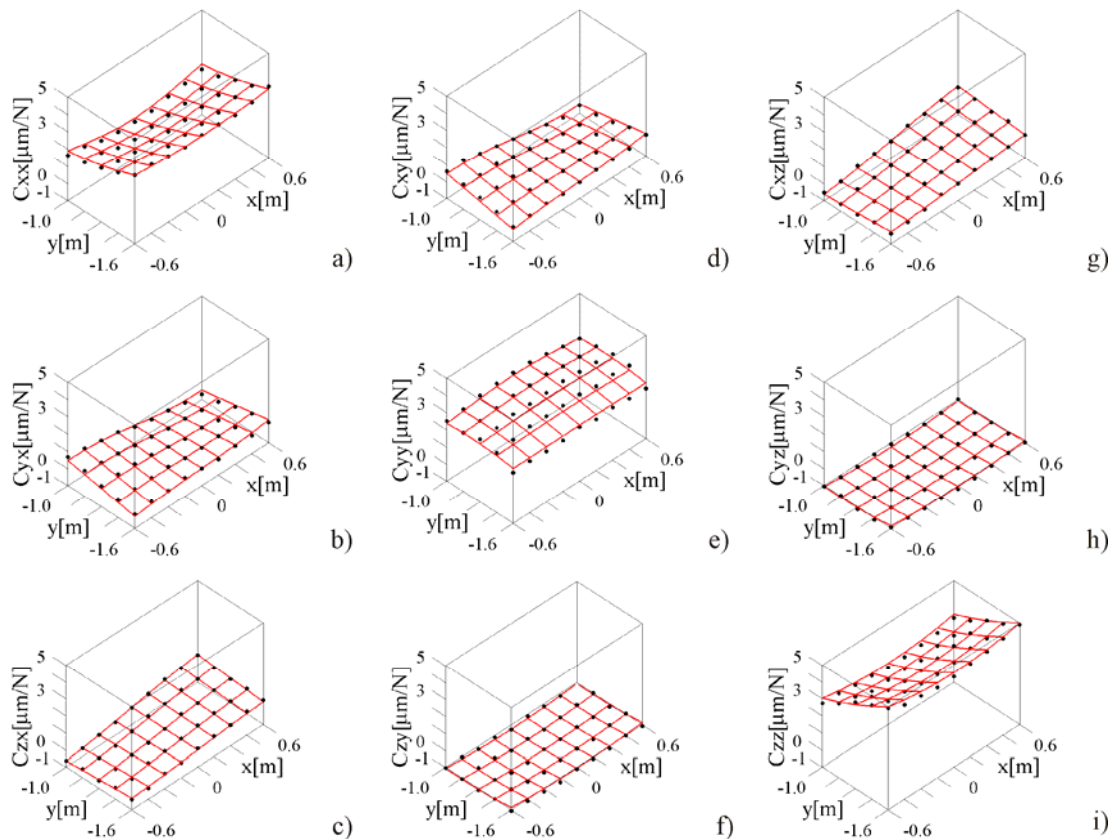
Figure 13. Distributions of calculated and experimentally determined compliances in the Z_M=0 plane
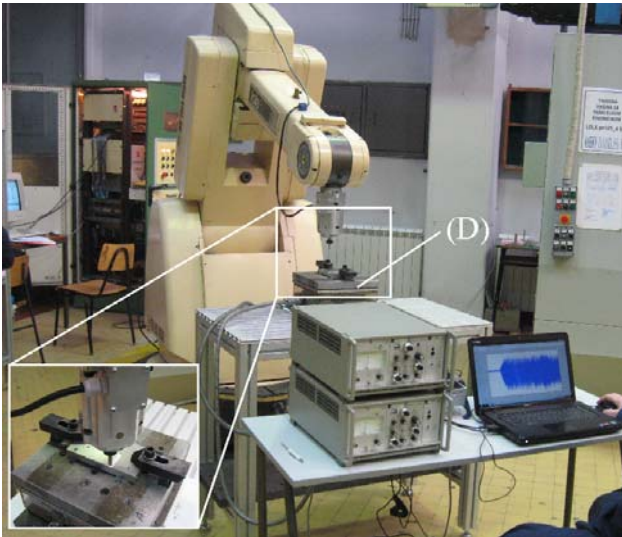
Figure 14. Robot milling tests

Figure 15 shows measured dynamic forces in the feed normal, i.e., the Y_M direction. To observe the static force component, *Fystat,* the force signal was filtered with a cut off frequency of f_c=50Hz. As it can be noticed a constant static force level is approximately *Fystat* =100 N.

The machined flute is displayed in Figure 16 from which it can be seen that in the Y_M direction the deviation from the correct path is about 0.3 mm. For the static force of approximately *Fystat*=100 N, Figure 15, the calculated displacement from the analytically determined compliance from Figure 5 is 0.23 mm, while the calculated displacement from the experimentally determined compliance, Figure 13, is approximately 0.29 mm. From this simple milling test it can be readily noticed that the calculated displacement from the experimentally determined compliance is approximately equal to the measured tool path deviation on the workpiece. The calculated displacement based on the analytically determined compliance is nearly three quarters of the real displacements.
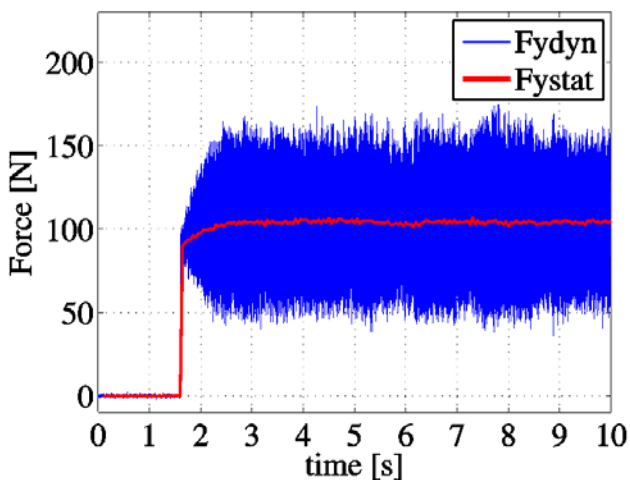
Figure 15. Measured force in the Y_M-direction
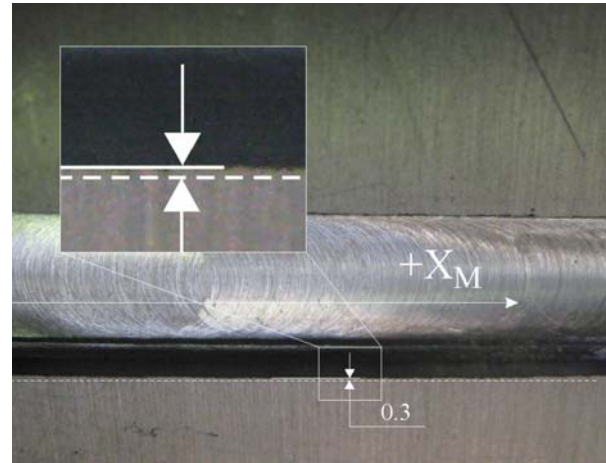
Figure 16. Machined flute

6.   CONCLUSION

The paper presents analytically- and experimentally-based compliance identification and analysis of a 5-axis vertical articulated machining robot. By expanding the conventional analytical approach to the mapping of joint compliances into the robot's Cartesian space compliance, it has been shown that it is possible to analyze the impact of each individual joint's compliance on the robot's Cartesian space compliance. This is of crucial importance, because it can be useful for a robot manufacturer's experts in the design of specialized machining robots. Also, a satisfactory correlation between the analytically- and experimentally-based Cartesian compliances indicates that the analytical approach is efficient in identifying the Cartesian space robot compliance, considering that only five experiments are sufficient to identify the joint compliances. However, the identification of joint compliances based on experimentally determined Cartesian space compliances gives better results since many tests are performed in different robot configurations. A suitable model of the process forces and the expanded compliance model proposed in this paper also enable the development of virtual robotic machining systems for further research. The present research has laid the foundation for an advanced design method for machining robots as well as for the development of strategies for real-time tool tip displacement compensation based on captured process forces which are already the subject of current research.

REFERENCES

[1] Abele, E., Kulok M. and Weigold, V.: Analysis of a machining industrial robot, in: *Proceedings of the 10th International Scientific Conference on Production Engineering,* 2005, Lumbarda, pp. II 1-11.

[2] Pan, Z. and Zhang H.: Robotics machining from programming to process control: a complete solution by force control, Industrial Robot: An International Journal, Vol. 35, No. 5, pp. 400-409, 2008.

[3] Abele, E., Rothenbucher, S. and Weigold, M.: Cartesian compliance model for industrial robots using virtual joints, Production Engineering. Research and Development, Vol. 2, No. 3, pp. 339-343, 2008.

[4] Alici, G. and Shirinzadeh, B.: Enhanced stiffness modeling, identification and characterization for robot manipulators, IEEE Trasanctions on Robotics, Vol. 21, No. 4, pp. 554-564, 2005.

[5] M., Stelzer, O., Von Stryk, E., Abele, J., Bauer and M., Weigold, High speed cutting with industrial robots: Towards model based compensation of deviations, in: *Proceedings of Robotik*, Munich, pp. 143-146, 2008.

[6] Milutinovic, D., Glavonjic, M., Zivanovic, S., Dimic, Z. and Slavkovic, N.: Development of robot based reconfigurable machining system, in: *Proceedings of the 33rd Conference on Production Engineering of Serbia*, 2009, Belgrade, pp. 151-155.

[7] Milutinovic, D., Glavonjic, M., Slavkovic, N., Dimic, Z., Zivanovic, S., Kokotovic, B. and Tanovic, Lj.: Reconfigurable robotic machining system controlled and programmed in a machine tool manner, International Journal of Advanced Manufacturing Technology, Vol. 53, No. 9-12, pp. 1217-1229, 2011.

[8] Abele, E., Weigold, M. and Rothenbucher, S.: Modeling and identification of an industrial robot for machining applications, Annals of the CIRP, Vol. 56, No. 1, pp. 387-390, 2007.

[9] Hudgens, J.C., Hernandez, E and Tesar, D.: A compliance parameter estimation method for serial manipulator DSC, Applications of Modeling and Identification to Improve Machine Performance, ASME, Vol. 29, pp. 15–23, 1991.

[10] Milutinovic, D.: Universal compliant device based on SCARA concept, Robotics and Computer-Integrated Manufacturing, Vol. 13, No. 4, pp. 319-321, 1997.

[11] http://www.staubli.com/en/robotics/robot-solution-application/high-speed-machining-robot/, date: 6 October 2012.

[12] Lee, R.S. and She, C.H.: Developing a postprocessor for three types of five-axis machine tools, The International Journal of Advanced Manufacturing Technology, Vol. 13, No. 9, pp. 658-665, 1997.

[13] Affouard, A., Duc, E., Lartigue, C., Langeron, J.M. and Bourdet, P.: Avoiding 5-axis singularities using tool path deformation, International Journal of Machine Tools and Manufacture, Vol. 44, No. 4, pp. 415-425, 2004.

[14] ISO 841:2001 Industrial automation systems and integration-Numerical control of machines-coordinate system and motion nomenclature.

[15] Craig, J.J.: *Introduction to Robotics: Mechanics and Control*, 2nd edition, Addison-Wesley, New York, 1989.

[16] Spong, M.W. and Vidyasagar, M.: *Robot Dynamics and Control*, John Wiley and Sons, New York, 1989.

[17] Tsai, L.W.: *Robot Analysis: the Mechanics of Serial and Parallel Manipulators*, Wiley, New York, 1999.

[18] Sciavicco, L. and Siciliano, B.: *Modelling and Control of Robot Manipulators*, 2nd edition, Springer-Verlag, London Berlin Heidelberg, 2000.

[19] Dumas, C., Caro, S., Garnier, S. and Furet, B.: Joint stiffness identification of six-revolute industrial serial robots, Robotics and Computer-Integrated Manufacturing, Vol. 27, No. 4, pp. 881-888, 2011.

ИДЕНТИФИКАЦИЈА И АНАЛИЗА ПОПУСТЉИВОСТИ У ДЕКАРТОВОМ ПРОСТОРУ РОБОТА ЗА ОБРАДУ ВЕРТИКАЛНЕ ЗГЛОБНЕ КОНФИГУРАЦИЈЕ

Никола Славковић, Драган Милутиновић, Бранко Кокотовић, Милош Главоњић, Саша Живановић, Kornel Ehmann

Примена индустријских робота вертикалне зглобне конфигурације за вишеосну обраду глодањем је ограничена на делове од мекших материјала ниже класе тачности. Основни разлог за ово је недовољна крутост серијске структуре робота која је неколико десетина пута мања од крутости CNC машина алатки. У раду је представљен метод експерименталне идентификације и анализе попустљивости 5-осног робота за обраду вертикалне зглобне конфигурације. За одређивање попустљивости робота у Декартовом простору коришћен је проширени конвенционални приступ који је базиран на експерименталној идентификацији попустљивости зглобова и Јакобијан матрици. Аналитичка анализа обухвата утицај попустљивости сваког зглоба понаособ на попустљивост робота у Декартовом простору. Експериментално одређивање попустљивости робота у Декартовом простору је извршено мерењем апсолутних помераја врха робота изазваних статичким силама у сва три Декартова правца, из којих су затим одређене попустљивости сваког зглоба.